Raman scattering in $Hf_xZr_{1-x}O_2$ nanoparticles

Richard D. Robinson, Jing Tang, Michael L. Steigerwald, Louis E. Brus, and Irving P. Herman*
Materials Research Science and Engineering Center, Columbia University, New York, New York 10027, USA
(Received 30 August 2004; published 10 March 2005)

Raman spectroscopy demonstrates that ~5 nm dimension $Hf_xZr_{1-x}O_2$ nanocrystals prepared by a nonhydrolytic sol-gel synthesis method are solid solutions of hafnia and zirconia, with no discernable segregation within the individual nanoparticles. Zirconia-rich particles are tetragonal and ensembles of hafnia-rich particles show mixed tetragonal/monoclinic phases. Sintering at 1200 °C produces larger particles (20–30 nm) that are monoclinic. A simple lattice dynamics model with composition-averaged cation mass and scaled force constants is used to understand how the Raman mode frequencies vary with composition in the tetragonal $Hf_xZr_{1-x}O_2$ nanoparticles. Background luminescence from these particles is minimized after oxygen treatment, suggesting possible oxygen defects in the as-prepared particles. Raman scattering is also used to estimate composition and the relative fractions of tetragonal and monoclinic phases. In some regimes there are mixed phases, and Raman analysis suggests that in these regimes the tetragonal phase particles are relatively rich in zirconium and the monoclinic phase particles are relatively rich in hafnium.

DOI: 10.1103/PhysRevB.71.115408 PACS number(s): 61.46.+w, 78.30.−j, 78.67.Bf, 64.70.Nd

I. INTRODUCTION

Hafnia (HfO_2) and zirconia (ZrO_2) are called twin oxides because of their similar chemical and physical properties. They are isostructural in the bulk[1] and this close correlation in properties is due to the identical valence states and nearly identical ionic radii for Hf and Zr. Still, there is slightly stronger bonding in Hf compounds relative to the analogous Zr compounds.[1,2] The dielectric constants of hafnia and zirconia at low frequency are both very high, very roughly 20;[3–5] this, along with their stability when in contact with Si, make them interesting candidates for insulating barriers in microelectronics.[3] First principles calculations give orientationally-averaged dielectric constants of 20 for zirconia and 16–18 for hafnia in this monoclinic phase, and much higher dielectric constants for the tetragonal phase, 47 and 70 respectively.[4,5]

Bulk hafnia and zirconia can each adopt three different crystal structures at ambient pressures, i.e., monoclinic, tetragonal and cubic. In the bulk, each oxide is stable in the monoclinic phase at room temperature and each transforms to tetragonal at high temperatures, the former at 1720 °C and the latter at 1170 °C.[6] At even higher temperatures, 2600 °C and 2370 °C, respectively, the tetragonal phases transform to the cubic phase. At room temperature, zirconia is stable in the monoclinic phase for dimensions $\gtrsim$100 nm, while nanometer-sized zirconia is stable in the tetragonal phase. The reported "critical size" below which the tetragonal phase is stable ranges from 9–30 nm.[7–10] The reason for the formation and stability of tetragonal zirconia nanocrystals is still uncertain, and has been attributed to one of several factors, including the lower surface free energy for the high temperature phase[7] and anionic vacancies that nucleate the tetragonal phase.[11,12] There have been relatively few studies on the polymorphs of hafnia, and particularly nanosized crystals.[13,14] The first extensive synthesis of tetragonal hafnia nanoparticles was reported recently by the authors, who also reported the first synthesis of hafnia-zirconia solid solution nanoparticles.[14] Solid solutions of hafnia-zirconia ($Hf_xZr_{1-x}O_2$) are of interest for several reasons, including the need to understand the mode structure of such mixed nanocrystals. This is still an issue in bulk mixed crystals. For instance, the question of possible two-mode behavior in bulk $Hf_xZr_{1-x}O_2$ has attracted much attention.[15]

For these binary oxides, six of the 18 normal modes are allowed Raman modes in the tetragonal phase (space group D_{4h}^{15}, $Z=2$) and 18 of the 36 normal modes are allowed Raman modes in the lower symmetry monoclinic phase (space group C_{2h}^{5}, $Z=4$). Many of the studies of Raman scattering of tetragonal zirconia present evidence for conflicting assignments of the observed Raman modes.[9,16–18] To our knowledge, there have been no previous Raman scattering studies on tetragonal hafnia nanoparticles or hafnia-zirconia nanoparticle solid solutions, other than a brief report by the present authors in Ref. 14. The present authors presented preliminary results regarding the Raman spectra of as-synthesized $Hf_xZr_{1-x}O_2$ nanocrystals excited by the 325-nm line from a He-Cd laser; Raman analysis was not possible with excitation at 488 and 514.5 nm by an argon-ion laser, because the background luminescence was too intense.

This paper reports on the Raman spectra of $Hf_xZr_{1-x}O_2$ nanocrystals over a range of composition, particularly for those small particles in the tetragonal phase. These spectra demonstrate that the particles are solid solutions of hafnia and zirconia, with no discernable segregation within the individual nanoparticles. A simple lattice dynamics model is used to explore how changes in the average cation mass and interatomic force constants with alloy composition affect the Raman-allowed mode frequencies. The minimization of background luminescence from these particles, which in many cases is needed to be able to observe the Raman spectrum, is also addressed. The control of luminescence in these and other nanocrystals can provide insight into the location and control of defects.

II. EXPERIMENTAL PROCEDURE

$Hf_xZr_{1-x}O_2$ nanoparticles were synthesized through a nonhydrolytic sol-gel synthesis. The appropriate amounts (dictated by the value of x) of Hf(iso-propoxide)$_4$, $HfCl_4$, Zr(iso-propoxide)$_4$ and/or $ZrCl_4$ were added, under argon, to degassed trioctylphosphine oxide (TOPO, which acts as both solvent for the reaction and surface ligand for the product nanocrystals). The reaction mixture was heated quickly to 350 °C and held at this temperature for 2 h with vigorous stirring. The reaction mixture was then cooled to ~60 °C and acetone was added to precipitate the hafnia nanoparticles. The precipitate was retrieved by centrifugation and washed several times with acetone to remove excess TOPO. The particles are capped with TOPO ligands and can be readily redispersed in hexane producing a colorless solution. Further details of these preparations can be found in Ref. 14.

Unless otherwise stated, before Raman analysis all as-synthesized particles were annealed at 600 °C for 1 h in air. Larger particles were obtained by sintering in air at temperatures up to 1200 °C for 1 h. The average nanoparticle size was determined by Debye Scherrer analysis of x-ray powder diffraction (XRD) scans, which were recorded on a Scintag X2 diffractometer using Cu Ka radiation ($\lambda = 1.54056$ Å) operating at 35 mA, 45 kV. The elemental composition of these nanoparticles was determined by inductively coupled plasma (ICP) analysis.

Raman scattering was performed in a backscattering configuration using the 488 nm and 514.5 nm lines of a continuous wave argon ion laser (Coherent Innova 100), and the 325 nm line of a helium-cadmium laser (Omnichrome), at room temperature unless otherwise stated. The beam was focused to a spot size of ~2 μm and all incident power was less than 1 mW, to minimize heating in these powder samples. A 0.6 m triple spectrometer (SPEX 1877, Triplemate) in subtractive configuration was used to collect and disperse the spectra, and a UV coated Si CCD array detector (SPEX Spectrum One) collected the spectra. Plasma lines were used to calibrate the 70 to 800 cm^{-1} frequency range (resolution ~2 cm^{-1}). All peak intensities and positions are the result of Lorentzian fitting. The luminescence from as-synthesized nanoparticles was monitored as a function of temperature in oxidizing (air or oxygen), reducing (forming gas: 95% N_2 +5% H_2), and presumably nonreactive (N_2) gas environments. The heat-treated particles were then reexamined at room temperature in the same gas environment. Any background due to luminescence was subtracted before determining peak shifts.

III. EXPERIMENTAL RESULTS

The synthesized particles were typically quasispherical nanocrystals with ≃3.8–5.5 nm dimensions, typically for $x < 0.46$, while those with $x > 0.46$ were typically nanorods with dimensions ~3 nm by ~8 nm, as shown by earlier transmission electron microscope (TEM) analysis.[14] Only the quasispherical nanocrystals were examined here.

The average particle size, as determined by XRD, did not change with heating up to 600 °C. Particle size began to increase noticeably around 900 °C. In the earlier work by the authors,[14] TEM showed that these particles are single crystals. Table I gives the size and Hf fraction x (obtained from ICP analysis) of particles examined by Raman scattering after annealing at 600 °C (3.8–5.5 nm dimension) and sintering in air at 1200 °C for 1 h (20–30 nm). Raman scattering was also examined for several particles sintered in air for 1 h at lower temperatures: 900 °C ($x = 0$, 8.4 nm; $x = 0.45$, 5.4 nm; $x = 0.46$, 7.2 nm) and 1000 °C ($x = 0.35$, 15.3 nm).

TABLE I. Sizes of $Hf_xZr_{1-x}O_2$ nanoparticles analyzed after annealing at 600 °C or sintering at 1200 °C, both for 1 h in air. x is from ICP measurements. Phases are also shown from XRD, with t for tetragonal and m for monoclinic. Particles were also sintered for 1 h in air at lower temperature: 900 °C ($x = 0$, 8.4 nm; $x = 0.45$, 5.4 nm; $x = 0.46$, 7.2 nm) and 1000 °C ($x = 0.35$,15,3 nm).

	Particles annealed at 600 °C		Particles sintered at 1200 °C	
Particle type	Size (nm)	Phase from XRD	Size (nm)	Phase from XRD
ZrO_2	3.8	t	20.8	m
$Hf_{0.12}Zr_{0.88}O_2$	4.8	t	26.8	m
$Hf_{0.19}Zr_{0.81}O_2$	5.1	t	26.2	m
$Hf_{0.35}Zr_{0.65}O_2$	4.6	t	23.1	m
$Hf_{0.45}Zr_{0.55}O_2$	4.3	t	26.1	m
$Hf_{0.46}Zr_{0.54}O_2$	4.1	$t+m$	23.6	m
$Hf_{0.75}Zr_{0.25}O_2$	5.1	$t+m$	19.9	m
HfO_2	5.5	$t+m$	29.5	m

There was strong background luminescence when all as-synthesized nanoparticles were excited with sub-bandgap radiation at 488 and 514.5 nm. The emission was ~200 nm broad, starting at the excitation wavelength, and prevented obtaining a Raman spectrum. This luminescence was absent or weak enough with 325-nm excitation in some (3.7 nm HfO_2, 5.5 nm HfO_2, 4.3 nm $Hf_{0.45}Zr_{0.55}O_2$, and 4.6 nm $Hf_{0.35}Zr_{0.65}O_2$) but not all particles.[14]

Heating as-synthesized particles to 150 °C for 10 min in air decreased room-temperature luminescence by 40–70% ($\lambda = 514.5$ nm), but no change was seen after heating under these conditions in either N_2 or forming gas. Heating at higher temperature and longer times in air or O_2 decreased emission even more. All particles heated to 600 °C for 1 h in air produced Raman spectra with no interfering background emission at any of these three excitation wavelengths. The luminescence intensity of as-synthesized particles measured in air decreased by 20–70% after treatment by an oxygen plasma for 30 min.

The Raman spectra of HfO_2, ZrO_2, and several $Hf_xZr_{1-x}O_2$ nanoparticles taken at room temperature ($\lambda = 514.5$ nm) after annealing at 600 °C in air (Table I) are shown in Fig. 1. The peak frequencies of the six modes that are prominent for the $x < 0.46$ particles—the six tetragonal modes—are labeled T1–T6 in Fig. 1 and are plotted in Fig. 2 vs x. At each x examined, the mode structure in the spectra of particles sintered at or below 1000 °C (Table I caption) was

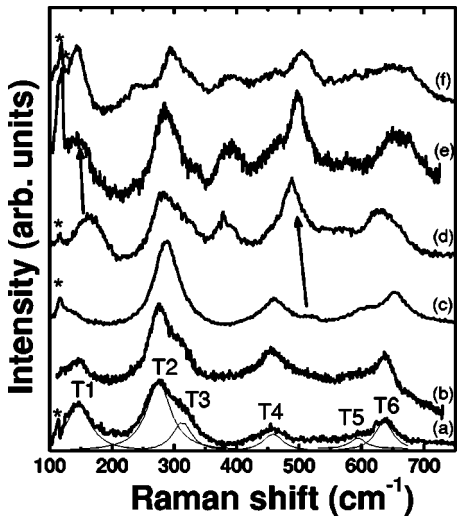

FIG. 1. Room temperature Raman spectra of $Hf_xZr_{1-x}O_2$ nanoparticles after heating at 600 °C in air for 1 h, taken with at $\lambda = 514.5$ nm: (a) ZrO_2, (b) $Hf_{0.12}Zr_{0.88}O_2$, (c) $Hf_{0.45}Zr_{0.55}O_2$, (d) $Hf_{0.46}Zr_{0.54}O_2$, (e) $Hf_{0.75}Zr_{0.25}O_2$, and (f) HfO_2. The Lorentzian fits of the peaks are shown only in (a). Peaks labeled T1–T6 are the six tetragonal phase first order Raman modes. The two arrows point from monoclinic phase peaks in spectra of lower x to the same peaks at higher x. Plasma lines from the laser are denoted by an asterisk.

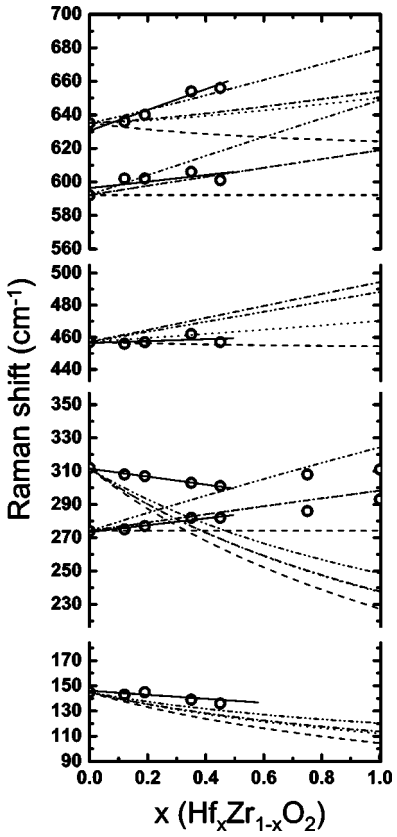

FIG. 2. Measured frequencies of the tetragonal modes of the $Hf_xZr_{1-x}O_2$ nanoparticles from Fig. 1 (circles fit to a solid line), compared to model predictions. Model predictions include assuming linear mass averaging only (– – – lines), and mass scaling with force constant scaling of all six force constants of zirconia by a factor of $1+0.09x$ (· · ·), similar scaling of only the four Zr-O interplane force constants (– · – · –), and scaling of only these four force constants by a factor of $1+0.2x$ (– · · – · · –). The results for $1+0.09x$ scaling of the four or all six force constants nearly overlap, except for the T4 mode. The modes are T1–T6 from bottom to top. (Note the measured shifts of T3 exceed those of T2 for all x.)

similar to the corresponding structure in Fig. 1 (but is not shown). Figure 3 shows the Raman spectra for the ~20–30 nm dimension particles after sintering at 1200 °C (Table I).

IV. DISCUSSION

A. Background emission

With 514.5 nm excitation at room temperature, luminescence decreased greatly after either heating to only 150 °C in oxygen-containing environments or exposure to oxygen plasmas, but not after heating in forming gas. This suggests that oxygen is removing bulk or surface oxygen deficiencies or defects, or is reacting with the surface ligands or other defects that luminesce. After treatment at 600 °C, the background luminescence is weaker than the Raman scattering.

When the as-synthesized particles were excited at 325 nm, relatively low levels of luminescence were observed; this luminscence did not interfere with Raman measurements. (See also Ref. 14.) Note the band gap in bulk hafnia-zirconia alloys is ~5–6 eV (~200–250 nm) and is expected to be no smaller than this in hafnia-zirconia nanoparticles. Therefore, the 325, 488, and 514.5 nm excitations are all below the band gap.

B. Raman spectra

The room temperature Raman spectrum of the small zirconia nanoparticles in Fig. 1 (3.8 nm, annealed at 600 °C) has six peaks, labeled T1–T6 for increasing mode frequency (with peaks T2 and T3 overlapping); these six peaks are a signature of the tetragonal phase. These tetragonal peaks are also the only ones seen for $Hf_{0.12}Zr_{0.88}O_2$ nanoparticles. For $x > 0.45$, additional peaks are seen due to monoclinic-phase modes. A very weak monoclinic peak is seen for $Hf_{0.45}Zr_{0.55}O_2$ nanoparticles at 513 cm^{-1} (see the tail of the right arrow), which is likely due to a mode in the monoclinic phase.[1] More dominant monoclinic peaks are seen for larger x. This suggests that only the tetragonal phase is present for the smaller $x(<0.45)$, while there is evidence of both tetragonal and monoclinic phases for larger $x(>0.45)$ and for hafnium nanoparticles. This likely means that there is a mixture of tetragonal and monoclinic particles and not mixed phases within a particle, because TEM has shown that each particle is a single crystal. Raman spectra were taken at various points in the probed powder, because the employed Raman diagnostic probes a lateral dimension of about 2 μm. These spectra of different spots showed no essential differences.

The Raman mode frequencies vary with hafnium content. Also, no pure zirconia or pure hafnia Raman modes are observed for these alloy nanoparticles. Both observations dem-

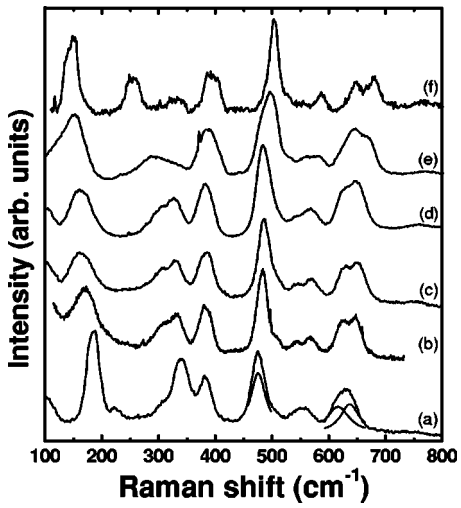

FIG. 3. Room temperature Raman spectra of $Hf_xZr_{1-x}O_2$ nanoparticles after sintering at 1200 °C in air for 1 h, taken with at $\lambda = 514.5$ nm: (a) ZrO_2, (b) $Hf_{0.12}Zr_{0.88}O_2$, (c) $Hf_{0.45}Zr_{0.55}O_2$, (d) $Hf_{0.46}Zr_{0.54}O_2$, (e) $Hf_{0.75}Zr_{0.25}O_2$, and (f) HfO_2. The Lorentzian fits of the M12 (475 cm^{-1}), M16 (616 cm^{-1}), and M17 (637 cm^{-1}) peaks that are used for composition analysis are shown only in (a).

onstrate that the particles are solid solutions with at least fairly good mixing of Hf and Zr, with no discernable segregation of hafnia and zirconia within the individual nanoparticles. (Such mixing cannot be determined by usual powder XRD because of the nearly identical lattice constants of hafnia and zirconia.) This also indicates there are no distinct, pure hafnia and pure zirconia particles for x not equal to 0 or 1. The dependence of the tetragonal mode frequencies are modeled below on the basis of this mixing. Also, particle compositions are determined below on the basis of this mixing and the consequent dependence of the mode frequency on x.

Not all 18 modes of the monoclinic phase can be identified in the Raman spectra of the hafnia-rich particles in Fig. 1, in part because of the peak broadening for these very small particles.[19] The assignments of the stronger monoclinic modes M1-M18 are now presented. (They are as in Ref. 1, but with M7 and M8 reversed and M16 and M17 reversed, so the frequencies monotonically increase.) The strong and sharp modes M2 near 135 cm^{-1} and M4 near 150 cm^{-1} in pure monoclinic hafnia overlap the T1 peak. The observed shoulder at 240 cm^{-1} in the hafnia particles here is due to the medium strong hafnia M6-M8 peaks at 242, 256, and 270 cm^{-1}. For mixed tetragonal/monoclinic phases, spectral analysis of T2 and T3 could be weakly affected by these peaks and by the hafnia M9 mode near 336 cm^{-1}. Strong hafnia monoclinic peaks near 384 and 398 cm^{-1} (M10 and M11) are seen as a broad peak near 390 cm^{-1} in the mixed phases. The hafnia M12 peak at 503 cm^{-1} is very strong, and it is seen here as a peak for $x \geq 0.46$ nanoparticles, which has a low frequency shoulder due to T4. The strong and broad hafnia modes M16 (642 cm^{-1}) and M17 (672 cm^{-1}) are seen in Figs. 1(d)–1(f) to overlap T6.

No evidence of two-mode behavior is seen for any modes; evidence of some two-mode behavior was seen at low temperature for bulk monoclinic $Hf_xZr_{1-x}O_2$.[15] Given the large width of the peaks for these very small particles, it is unlikely that any two-mode behavior could be observed.

Zirconia-rich particles ($x < 0.45$) sintered at 900 °C (5–8 nm dimension) have only tetragonal phase Raman peaks, while the spectra of the even larger nanoparticles ($x \leq 0.75$) sintered at 1200 °C (20–30 nm) have only monoclinic peaks (Fig. 3). This suggests the critical diameter for the transition from the tetragonal to monoclinic phases is roughly between 6–8 and 20–30 nm in this composition range. In the one sintering run at 1000 °C, $Hf_{0.35}Zr_{0.65}O_2$ nanoparticles grew to 15.3 nm. The room temperature Raman spectrum of these nanoparticles has only tetragonal peaks, so the critical diameter for $x = 0.35$ is between 15 and 23 nm.

The Raman identifications of tetragonal (Fig. 1), monoclinic (Fig. 3), and mixed phases (Fig. 1) were confirmed by XRD analysis (Table I).

Using Raman scattering for quantitative analysis

Peak T2 seems relatively unaffected by monoclinic peaks and peak M12 seems to be relatively unaffected by tetragonal peaks, and they are both strong, making them good candidates for use in composition and phase analysis.

a. Determining composition. Raman scattering can determine composition, and as such is a nondestructive alternative to ICP analysis. Raman scattering has been used to determine the composition in bulk, monoclinic $Hf_xZr_{1-x}O_2$ by tracking the Raman shifts of two of the higher frequency peaks that have been shown to vary smoothly and linearly with composition.[20,21] Although, XRD analysis can be used to determine the composition in bulk $Hf_xZr_{1-x}O_2$ by measuring the lattice spacing, this requires high-resolution XRD because the lattice constants of HfO_2 and ZrO_2 are nearly equal.[20] Such analysis is much more difficult for the alloy nanoparticles because of peak broadening in the nanoparticles.

Figure 2 shows that the T2 peak frequency varies fairly linearly with x, and so composition could be determined by linearly interpolating between the measured mode 2 frequencies for the zirconia ($x = 0$, 274 cm^{-1}) and hafnia ($x = 1$, 293 cm^{-1}) particles. Table II shows the agreement between the ICP and Raman scattering is quite good and within $\pm$ 0.1. In principle, variations in mode shifts with diameter could be significant in using such methods to determine composition in alloy particles. (All of the tetragonal particles have about the same diameter here.)

The M12 peak frequencies for samples annealed at 600 °C show a clear variation with composition: $Hf_{0.46}Zr_{0.54}O_2$: 487 cm^{-1}, $Hf_{0.75}Zr_{0.25}O_2$: 502 cm^{-1}, and HfO_2: 505 cm^{-1}. This monoclinic-phase peak M12 was used to analyze composition in the larger (20–30 nm), monoclinic-phase particles that had been heated at 1200 °C (Fig. 3). Linearly interpolating between the frequencies measured for these zirconia and hafnia nanoparticles (475 and 503 cm^{-1}), assuming single-mode behavior,[15] gives x in Table II. This was also done using peaks M16 and M17 (616 and 637 cm^{-1} in zirconia, and 641 and 675 cm^{-1} in hafnia),

TABLE II. Comparison of composition determined from Raman scattering to that from ICP (given as x in $Hf_xZr_{1-x}O_2$) for tetragonal particles (annealed at 600 °C; using peak T2) and monoclinic particles (sintered at 1200 °C; using either peak M12 or peaks M16 and M17). For $Hf_{0.46}Zr_{0.54}O_2$ particles annealed at 600 °C (mixed phase), $x_m=0.43$ from the monoclinic peak 12. See Table I for particle dimensions.

	Particles annealed at 600 °C	Particles sintered at 1200 °C	
Particle type	x_t from tetragonal peak 2	x_m from monoclinic peak 12	x_m from monoclinic peaks 16 and 17
ZrO_2	0.00	0	0
$Hf_{0.11}Zr_{0.89}O_2$		0.07	0.02
$Hf_{0.12}Zr_{0.88}O_2$	0.05	0.04	0.01
$Hf_{0.19}Zr_{0.81}O_2$	0.16	0.07	0.12
$Hf_{0.21}Zr_{0.79}O_2$	0.10	0.00	0.19
$Hf_{0.35}Zr_{0.65}O_2$	0.42	0.25	0.32
$Hf_{0.45}Zr_{0.55}O_2$	0.42	0.39	0.42
$Hf_{0.46}Zr_{0.54}O_2$	0.32	0.36	
$Hf_{0.75}Zr_{0.25}O_2$	0.63	0.71	0.96
HfO_2	1.00	1	1

as in Ref. 21 (by averaging x determined using either M16 or M17). There is poor agreement with the ICP results for $x<0.2$ and good agreement for higher x using the M12 peak and for x between 0.2 and 0.45 when using the M16 and M17 peaks.

b. Determining the fractions of tetragonal and monoclinic phases. Peaks T2 and M12 can be used to determine the fractions of tetragonal and monoclinic phases, f_t and f_m (with $f_t+f_m=1$), for any x, and serve as an alternative to XRD. For $x\geqslant 0.46$ [Figs. 1(d)–1(f)], the ratios of the peak intensities and integrated areas of M12 and T2 are 1.3 and 2.2 for the $x=0.46$ particles and 1.7 and 2.0 for the $x=0.75$ particles. Analysis of the XRD spectrum gives the ratio of monoclinic to tetragonal phase of 1.9 for the $x=0.46$ particles and 1.0 for the $x=0.75$ particles, so the M12 and T2 peaks are very roughly the same strength for the same amount of monoclinic and tetragonal material probed at 514.5 nm. In contrast, Kim *et al.*[22] claim that monoclinic zironica has a stronger Raman spectra than tetragonal zirconia, on the basis of the T1 peak near 148 cm^{-1} and the monoclinic peaks from 180–192 cm^{-1} (M2–M4) peaks, which are not resolvable for the very small particles here.

c. Evaluating possible different compositons in different phases. In the mixed phase solid solution samples, x determined by ICP is an average of both phases. It is possible that the hafnium fractions in the tetragonal and monoclinic phase particles, x_t and x_m, are different; either x_t and x_m could be $<x$ and the other $>x$—yet still with $x_tf_t+x_mf_m=x$. Raman scattering is well suited to see if this occurs (Table II). (Also, x_t and x_m, could be averaged values for each phase and there could be dispersion about these averages for each—but this is more difficult to address.) For the $x=0.46$ mixed phase particles previously heated to 600 °C, x_t (using the T2 peak) is 0.32 and x_m (using the M12 peak) is 0.43 (see Table II caption). For the $x=0.75$ mixed phase particles previously heated to 600 °C, x_t (using the T2 peak) is 0.63 and x_m (using the M12 peak) is 0.96. In both cases the tetragonal phase seems to be relatively rich in zirconium and the monoclinic phase relatively rich in hafnium. This is reasonable because the monoclinic phase appears in these smaller particles when the hafnium fraction increases. As the particles grow during heating, one might expect x_t and x_m to both approach x (and x_m to decrease here). For the $x=0.46$ and 0.75 particles previously sintered at 1200 °C (all monoclinic), $x=x_m$ (using the M12 peak) is 0.36 and 0.71 respectively, and so both cases show this trend. (Note that if the different phases have different compositions, perhaps these nanoparticles should not be termed $Hf_xZr_{1-x}O_2$ particles, although these mixed phase particle ensembles can still be characterized by an average hafnia fraction x.)

C. Lattice dynamics model

The simple linear chain model developed by Bouvier and Lucazeau in Ref. 18 to characterize and assign the six allowed tetragonal Raman modes in zirconia nanoparticles is slightly modified and used here to examine the variations of the mode frequencies in tetragonal $Hf_xZr_{1-x}O_2$ nanoparticles with composition (3.8–5.5 nm, annealed at 600 °C). For the solid solution nanoparticles, the model uses masses and force constants that are averaged over composition. In the original linear lattice chain model for zirconia, each atom in the primitive cell is assigned to one of six planes successively containing Zr, O, O, Zr, O, O, and these planes are coupled through interactions with differerent force constants, as outlined in the Appendix here. Reference 18 used this model to deduce that the (T1,T2,T3,T4,T5,T6) modes have $(E_g,E_g,B_{1g},E_g,A_{1g},B_{1g})$ symmetry. The force constants C_{d1} and C_{d2} represent the two different effective stretching interactions of the Zr and O atom planes and can be thought of as projections of the real force constants on the axis normal to the planes, and C_w describes non-nearest neighbor contributions and angular interactions that are effectively described as stretching interactions of two O planes. The frequency of the A_{1g} mode is determinied by $C_{d1}+C_{d2}$, while the two B_{1g} modes are determined by C_{d1}, C_{d2}, and C_w. Analogous shear interactions are characterized by the C^s_{d1}, C^s_{d2}, and C^s_w that describe the three E_g modes. The six force constants for tetragonal zirconia were determined from the Raman shifts of the T1-T6 modes of the 3.8 nm zirconia particles, and are given in the Appendix.

In the alloy model, the average cation mass $\langle m_{\text{cation},1}(x)\rangle = (1-x)m_{Zr}+xm_{Hf}$ replaces m_{Zr}, where m_{Zr} and m_{Hf} are the masses of zirconium and hafnium (91.22 and 178.49 amu, respectively), to model the changes in mass with composition. Such mass scaling is not unreasonble with one-mode alloy behavior. The force constant for the Hf-O stretch is about 9% higher than the Zr-O stretch in diatomic molecules. [This is determined using the HfO and ZrO vibrational ener-

gies, which are almost exactly the same, $\sim 969\ \mathrm{cm}^{-1}$,[23–25] and their (different) reduced masses.] The force constants for zirconia were either used directly (as a base case to examine mass effects only) or the zirconia constants were multiplied by $1+0.09x$ to provide scaling to hafnia.

The model was tested using the mode assignments for the T1-T6 modes zirconia from Bouvier and Lucazeau, and alternatively, earlier proposed and different symmetry assignments of the six modes: $(B_{1g},E_g,B_{1g},E_g,A_{1g},E_g)$,[16] $(E_g,B_{1g},A_{1g},E_g,B_{1g},E_g)$,[26] $(B_{1g},E_g,A_{1g},E_g,B_{1g},E_g)$,[27] and $(E_g,A_{1g},B_{1g},E_g,B_{1g},E_g)$.[28] The assignments from Ref. 18 were the only ones to yield reasonable results for the ZrO_2 and $Hf_xZr_{1-x}O_2$ nanoparticle mode models. Assumption of the other mode assignments led to negative or imaginary force constants. This is noted, although it is not proof that the Ref. 18 assignments are correct for zirconia or the alloys. This assignment has been confirmed for zirconia by the lattice dynamics study of Ref. 29. Another strength of the Bouvier and Lucazeau assignment is that it is based in part on their observation of anticrossing of the two lowest frequency modes (T1 and T2) at elevated pressure, which indicates they have the same symmetry. The frequency of the T2 mode decreased with pressure, and was identified as the soft mode leading to the transition to an intermediate tetragonal structure preceding the transformation to the cubic structure.[30]

Figure 2 compares the experimental Raman shifts with the lattice model predictions, with the model using compositionally-averaged cation masses, either with or without the scaled force constants described above. This comparison should be evaluated seriously only for x up to 0.45—although some data are provided for larger x—because of uncertainties with overlapping monoclinic modes for larger x. With such scaling of the cation mass and of all six force constants, the model accounts for modes 1, 2, and 5 fairly well. Model improvements could come from different scaling of the cation masses or force constants.

From Eqs. (A1)–(A3), one E_g mode (mode 2) and the A_{1g} mode (mode 5) do not depend on cation mass, because the cation does not move in the vibration. The increase of force constants with x accounts for the observed slow increase of their frequencies with x. For the other four modes, this mass variation decreases the frequency by a factor between 1 and $[(m_{Zr}+2m_O)/(<m_{cation}(x)>+2m_O)]^{1/2}$ (which is <1), while bond stiffening tends to increase it with x. This mass factor is nearly 1 for modes 4 and 6, and nearer the lower limit for modes 1 and 3. With the stated force scaling, the predicted decrease of frequency with x is faster than the observed decrease for modes 1 and 3, and, the predicted increase with x is slower than the observed increase for mode 6, which suggest the need for a slower mass variation and/or a faster stiffening with x. Indeed, averaging the reciprocals of the cation masses $\langle m_{cation,2}(x)\rangle = 1/[(1-x)/m_{Zr}+x/m_{Hf}]$ gives a slower mass variation, but this change has a relatively minor effect.

Only mode 4 near 460 cm^{-1} is significantly affected when instead of scaling all six force constants, only the four Zr-O interplane force constants $(C_{d1},C_{d2},C^s_{d1},C^s_{d2})$ are scaled and the two effective interactions between the O-O planes (C_w,C^s_w) are not. Then this mode and therefore all three E_g modes are well described by the model. This again suggests consistency with (though not proof of) the assignment that the two lowest modes have this same symmetry.

The measured frequencies are higher than predictions for modes 3 and 6, the two B_{1g} modes, with either model using $1+0.09x$ force constant scaling. This could indicate different scalings of several of the force constants (some should scale much faster than assumed here on the basis of the different IR frequencies in zirconia and hafnia[4,5]), an incorrect mode assignment, or an inherent weakness of this simple lattice plane model with averages to account for the composition changes. Figure 2 also shows the faster $1+0.2x$ scaling of the four Zr-O interplane force constants, which explains mode 6 better. There is no indication of a decrease of mode frequency in tetragonal particles as x approaches 0.46 (and the transition to the monoclinic phase at higher x) beyond that of the model expectations (for every model that includes the scaling of the force constants), and as such there is no evidence of a soft mode.

Use of such a simple lattice model presupposes bulklike material. For successively smaller particles, the Raman spectra change for several reasons and each Raman mode can change differently. A lattice model can account for some, but not all, of these effects. Strain can change with particle size due to surface tension, defects, and so on, and this can be incorporated as force constants that change with size. Phonon dispersion, and consequently phonon confinement, is different in smaller particles and this and other factors, including particle shape, are less easily incorporated into a simple lattice model. For very small particles, even small dispersion in particle size can strongly affect the Raman spectrum.[19] For example, in ceria nanoparticles, the cubic Raman peak becomes more redshifted and broader for smaller particles sizes because of strain, phonon confinement, and size dispersion.[19] The decrease in the Raman peak linewidth of zirconia nanoparticles from room temperature to 96 K, measured in Ref. 10, suggests that phonon confinement may not make the dominant contribution to the linewidths observed here, at least for zirconia nanoparticles. In any case, such analysis of the effect of size is beyond the scope of the present treatment. (All of the tetragonal particles described in Figs. 1 and 2 have about the same dimension, so no scaling with diameter is needed for the model presented in Fig. 2.)

V. CONCLUDING REMARKS

Raman scattering demonstrates that the $Hf_xZr_{1-x}O_2$ particles are solid solutions of hafnia and zirconia, with no discernable segregation within the nanoparticles and there are no distinct hafnia and zirconia particles. A simple lattice dynamics model with composition-averaged cation mass and scaled force constants is used to understand how the Raman mode frequencies vary for these alloys. Background luminescence from these particles is minimized after oxygen treatment, suggesting possible oxygen defects in the as-prepared particles. Raman scattering can also provide semiquantitative, nondestructive analysis of composition and the

fraction of each phase. In some regimes there are mixed phases, and Raman analysis suggests that in these regimes the tetragonal phase particles are relatively rich in zirconium and the monoclinic phase particles are relatively rich in hafnium.

ACKNOWLEDGMENTS

This work was supported primarily by the MRSEC Program of the National Science Foundation under Grant Number DMR-0213574 and by the New York State Office of Science, Technology and Academic Research (NYSTAR), and also by the Ford Foundation and the NSF IGERT Program Grant Number DGE-9972892. The authors would like to thank Siu-Wai Chan for discussions and Jason Fabbri for help in synthesizing the particles and analyzing them by XRD.

APPENDIX

In the Bouvier and Lucazeau model of tetragonal zirconia[18] the cell is modeled as six planes successively containing Zr, O, O, Zr, O, O (planes 1 to 6). The force constant C_{d1} represents the effective stretching interactions of Zr planes with the nearest neighbor O atom planes (1-2, 3-4, 4-5 and those with adjacent cells) and C_{d2} represents the effective stretching interactions of Zr planes with the next-nearest neighbor O atom planes (1-3, 2-4, 4-6 and those with adjacent cells). C_w describes non-nearest neighbor contributions and angular interactions and are effectively stretching interactions of pairs of next-nearest neighbor O planes (2-5, 3-6). The effective shearing interactions by the C^s_{d1}, C^s_{d2}, and C^s_w are force constants between the analogous pairs of planes.

The eigenfrequency ω of the A_{1g} mode is given by

$$M_O\omega^2(A_{1g}) - \alpha = 0, \tag{A1}$$

where $\alpha = C_{d1} + C_{d2}$ and M_O is the mass of an oxygen atom.

The eigenfrequencies of the two B_{1g} modes are given by

$$[M_{Zr}\omega^2(B_{1g}) - 2\alpha][M_O\omega^2(B_{1g}) - (\alpha + 2C_w)] - 2\beta^2 = 0, \tag{A2}$$

where $\beta = C_{d1} - C_{d2}$ and M_{Zr} is the mass of a zirconium atom.

The eigenfrequencies of the three E_g modes are given by

$$[M_O\omega^2(E_g) - \alpha^s]\{[M_{Zr}\omega^2(E_g) - 2\alpha^s][M_O\omega^2(E_g) - (\alpha^s + 2C^s_w)] - 2(\beta^s)^2\} = 0, \tag{A3}$$

where $\alpha^s = C^s_{d1} + C^s_{d2}$ and $\beta^s = C^s_{d1} - C^s_{d2}$.

In the current model the cation mass (above M_{Zr}) is replaced by the cation-averaged mass, and either the zirconia or cation-scaled force constants are used. The zirconia interplane force constants used here were fit to the measured Raman shifts of the T1-T6 modes of the 3.8 nm zirconia particles, 145, 274, 312, 457, 592, and 635, cm^{-1}, and were $C_{d1} = 2.33$, $C_{d2} = 0.99$, $C_w = 0.13$, $C^s_{d1} = 0.60$, $C^s_{d2} = 0.11$, and $C^s_w = 0.61$ N cm^{-1}, which are a bit different from those determined in Ref. 18.

*Corresponding author. Email address: iph1@columbia.edu

[1] P. E. Quintard, P. Barberis, A. P. Mirgorodsky, and T. Merle-Mejean, J. Am. Ceram. Soc. **85**, 1745 (2002).

[2] A. Ait-Ouali, S. Jandl, P. Marinier, J.-M. Lopez-Castillo, and A.-M. S. Tremblay, Phys. Rev. B **46**, 5183 (1992).

[3] G. D. Wilk, R. M. Wallace, and J. M. Anthony, J. Appl. Phys. **89**, 5243 (2001).

[4] X. Zhao and D. Vanderbilt, Phys. Rev. B **65**, 075105 (2002).

[5] X. Zhao and D. Vanderbilt, Phys. Rev. B **65**, 233106 (2002).

[6] F. Cardarelli, *Materials Handbook* (Springer, London, 2000).

[7] R. Garvie, J. Phys. Chem. **69**, 1238 (1965).

[8] R. Garvie, J. Phys. Chem. **82**, 218 (1978).

[9] E. Djurado, P. Bouvier, and G. Lucazeau, J. Solid State Chem. **149**, 399 (2000).

[10] P. Bouvier, E. Djurado, C. Ritter, A. J. Dianous, and G. Lucazeau, Int. J. Inorg. Mater. **3**, 647 (2001).

[11] R. Srinivasan, L. Rice, and B. H. Davis, J. Am. Ceram. Soc. **73**, 3528 (1990).

[12] E. Tani, M. Yoshimura, and S. Somiya, J. Am. Ceram. Soc. **66**, 11 (1983).

[13] S. J. L. Ribeiro, Y. Messaddeq, R. R. Goncalves, M. Ferrari, M. Montagna, and M. A. Aegerter, Appl. Phys. Lett. **77**, 3502 (2000).

[14] J. Tang, J. Fabbri, R. D. Robinson, Y. Zhu, I. P. Herman, M. L. Steigerwald, and L. E. Brus, Chem. Mater. **16**, 1336 (2004).

[15] C. Carlone, Phys. Rev. B **45**, 2079 (1992).

[16] A. Feinberg and C. H. Perry, J. Phys. Chem. Solids **42**, 513 (1981).

[17] P. Barberis, T. Merle-Mejean, and P. Quintard, J. Nucl. Mater. **246**, 232 (1997).

[18] P. Bouvier and G. Lucazeau, J. Phys. Chem. Solids **61**, 569 (2000).

[19] J. E. Spanier, R. D. Robinson, F. Zhang, S.-W. Chan, and I. P. Herman, Phys. Rev. B **64**, 245407 (2001).

[20] M. A. Krebs and R. A. Condrate, J. Am. Ceram. Soc. **65**, C144 (1982).

[21] A. R. West, *Solid State Chemistry and its Applications* (Wiley, Chichester, 1987), pp. 73–75.

[22] B.-K. Kim, J.-W. Hahn, and K. R. Han, J. Mater. Sci. Lett. **16**, 669 (1997).

[23] K. P. Huber and G. Herzberg, *Molecular Spectra and Molecular Structure: IV. Constants of Diatomic Molecules* (Van Nostrand Reinhold Co., New York, 1979).

[24] B. Simard, S. A. Mitchell, M. R. Humphries, and P. A. Hackett, J. Mol. Spectrosc. **129**, 186 (1988).

[25] A. Lesarri, R. D. Suenram, and D. Brugh, J. Chem. Phys. **117**, 9651 (2002).

[26] A. P. Mirgorodsky, M. B. Smirnov, and P. E. Quintard, J. Phys. Chem. Solids **60**, 985 (1999).
[27] C. Pecharroman, M. Ocana, and C. J. Serna, J. Appl. Phys. **80**, 3479 (1996).
[28] G.-M. Rignanese, F. Detraux, X. Gonze, and A. Pasquarello, Phys. Rev. B **64**, 134301 (2001).
[29] P. Bouvier, H. C. Gupta, and G. Lucazeau, J. Phys. Chem. Solids **62**, 873 (2001).
[30] P. Bouvier, V. Dmitriev, and G. Lucazeau, Eur. Phys. J. B **35**, 301 (2003).